



# HHS Public Access

Author manuscript

*Dev Cell*. Author manuscript; available in PMC 2015 December 22.

Published in final edited form as:

*Dev Cell*. 2014 December 22; 31(6): 722–733. doi:10.1016/j.devcel.2014.11.012.

## An Essential Role for Senescent Cells in Optimal Wound Healing through Secretion of PDGF-AA

Marco Demaria<sup>1</sup>, Naoko Ohtani<sup>2</sup>, Sameh A. Youssef<sup>3</sup>, Francis Rodier<sup>1,9</sup>, Wendy Toussaint<sup>4,10</sup>, James R. Mitchell<sup>4,11</sup>, Remi-Martin Laberge<sup>1</sup>, Jan Vijg<sup>5</sup>, Harry Van Steeg<sup>6,7</sup>, Martijn E.T. Dollé<sup>7</sup>, Jan H.J. Hoeijmakers<sup>4</sup>, Alain de Bruin<sup>3</sup>, Eiji Hara<sup>2</sup>, and Judith Campisi<sup>1,8,\*</sup>

<sup>1</sup>Buck Institute for Research on Aging, 8001 Redwood Boulevard, Novato, CA 94945, USA

<sup>2</sup>Division of Cancer Biology, The Japanese Foundation for Cancer Research, Koto-ku, Tokyo

135-8550, Japan <sup>3</sup>Department of Pathobiology, Dutch Molecular Pathology Center, Faculty of

Veterinary Medicine, Utrecht University, Utrecht 3509, the Netherlands <sup>4</sup>CGC Department of

Genetics, Erasmus Medical Center, Rotterdam 12306, the Netherlands <sup>5</sup>Department of Genetics,

Albert Einstein College of Medicine, 1301 Morris Park Avenue, Bronx, NY 10461, USA

<sup>6</sup>Department of Toxicogenetics, Leiden University Medical Center, Leiden 2318 NN, the

Netherlands <sup>7</sup>National Institute of Public Health and the Environment (RIVM), Antonie van

Leeuwenhoeklaan 9, Bilthoven 3721 MA, the Netherlands <sup>8</sup>Lawrence Berkeley National

Laboratory, Life Sciences Division, 1 Cyclotron Road, Berkeley, CA 94720, USA

### SUMMARY

Cellular senescence suppresses cancer by halting the growth of premalignant cells, yet the accumulation of senescent cells is thought to drive age-related pathology through a senescence-associated secretory phenotype (SASP), the function of which is unclear. To understand the physiological role(s) of the complex senescent phenotype, we generated a mouse model in which senescent cells can be visualized and eliminated in living animals. We show that senescent fibroblasts and endothelial cells appear very early in response to a cutaneous wound, where they accelerate wound closure by inducing myofibroblast differentiation through the secretion of platelet-derived growth factor AA (PDGF-AA). In two mouse models, topical treatment of senescence-free wounds with recombinant PDGF-AA rescued the delayed wound closure and lack of myofibroblast differentiation. These findings define a beneficial role for the SASP in tissue repair and help to explain why the SASP evolved.

---

© 2014 Elsevier Inc.

\*Correspondence: jcampisi@lbl.gov.

<sup>9</sup>Present address: Département de Radiologie, Radio-Oncologie et Médecine Nucléaire, Université de Montréal et CRCHUM, Montréal, QC H2L 2W5, Canada

<sup>10</sup>Present address: Departments of Molecular Biomedical Research, Vlaams Institute for Biotechnology, and Pulmonary Medicine, Ghent University, Ghent 9000, Belgium

<sup>11</sup>Present address: Department of Genetics and Complex Diseases, Harvard School of Public Health, 677 Huntington Avenue, Boston, MA 02115, USA

### SUPPLEMENTAL INFORMATION

Supplemental Information includes Supplemental Experimental Procedures and six figures and can be found with this article online at <http://dx.doi.org/10.1016/j.devcel.2014.11.012>.

## INTRODUCTION

Cellular senescence is a complex stress response whereby cells that are capable of proliferation lose this ability, essentially irreversibly (Campisi, 2013). Since its formal description >50 years ago (Hayflick and Moorhead, 1961), the senescence response has been implicated in two apparently disparate processes: tumor suppression and aging. There is now substantial evidence that the senescence growth arrest is indeed a formidable barrier to tumorigenesis, and mounting evidence indicates that an accumulation of senescence cells can drive phenotypes and pathologies associated with aging (Campisi, 2013). Thus, cellular senescence is likely an example of evolutionary antagonistic pleiotropy, being beneficial at young ages but detrimental at older ages (Campisi, 2003). Senescent cells most likely promote aging through their senescence-associated secretory phenotype (SASP): the increased expression and secretion of a suite of inflammatory cytokines, chemokines, growth factors, and proteases (Coppé et al., 2010a; van Deursen, 2014).

Although there are no strictly specific senescence markers, most senescent cells express the tumor suppressor p16<sup>INK4a</sup> (Ohtani et al., 2004), which prevents cell cycle progression from the G1 to S phases by inhibiting two cycle-dependent kinases, CDK4 and CDK6 (Sherr and Roberts, 1999). p16<sup>INK4a</sup> also increases with age and is a robust senescence marker in numerous mouse and human tissues (Krishnamurthy et al., 2004; Ressler et al., 2006), often coinciding with another prominent senescence marker, senescence-associated beta-galactosidase (SA- $\beta$ -gal) activity (Dimri et al., 1995). These and other markers have been used to understand the causes and consequences of cellular senescence in vivo.

Many stresses or stimuli induce a senescence response, including aging, genomic or epigenomic damage, and tissue injury. Senescent cells not only increase with age in multiple tissues, they are also prominent at sites of several age-related pathologies. These pathologies include atherosclerosis (Erusalimsky and Kurz, 2005), osteoarthritis (Martin and Buckwalter, 2003), chronic lung disease (Noureddine et al., 2011), and precancerous lesions (Collado et al., 2007). The SASP is thought to drive or exacerbate many of these pathologies. Recent results show that life-long elimination of senescent cells can prevent the development of certain age-related pathologies in a mouse model of segmental accelerated aging, strongly supporting the idea that senescent cells can be deleterious (Baker et al., 2011).

It remains unclear why senescent cells express a SASP given its prominent inflammatory components and mostly detrimental consequences (Freund et al., 2010). Of possible relevance to this puzzle, senescent cells were recently detected during embryogenesis, where they appear to play a nonessential role in optimizing the development of certain embryonic structures (Muñoz-Espín et al., 2013; Storer et al., 2013). Moreover, tissue repair and wound healing are impaired in old individuals (Guo and Dipietro, 2010), and the matrix metalloproteinases that comprise the SASP (Coppé et al., 2008, 2010b) were proposed to facilitate tissue repair by promoting collagen degradation, thereby limiting fibrosis (Jun and Lau, 2010; Krizhanovsky et al., 2008).

Tissue repair is an intricate process comprising four distinct overlapping phases: (1) hemostasis, (2) inflammation, (3) proliferation, and (4) remodeling. These phases are clearly evident during wound healing in the skin. In this tissue, wound closure occurs during the proliferation phase as a consequence of wound contraction (Midwood et al., 2004), which is due primarily to the formation of a newly synthesized granulation tissue and induction of specialized contractile fibroblasts termed myofibroblasts (Tomasek et al., 2002). Each phase is facilitated by soluble factors, some of which are known SASP factors.

To more precisely assess the physiological role of senescent cells *in vivo*, we created a mouse model (p16-3MR) in which senescent cells can be detected in living animals, isolated from tissues, and eliminated upon treatment with an otherwise ineffective drug. Here we show that senescent fibroblasts and endothelial cells appear at wound sites a few days after skin injury. These wound-associated senescent cells then promote optimal wound healing by secreting PDGF-A, a SASP factor, which promotes myofibroblast differentiation. These data support a positive role for senescent cells during tissue repair and help to explain why the SASP evolved.

## RESULTS

### The p16-3MR Mouse Model

To identify, isolate, and selectively kill senescent cells, we took advantage of the 3MR (trimodality reporter) fusion protein, which contains functional domains of a synthetic Renilla luciferase (LUC), monomeric red fluorescent protein (mRFP), and truncated herpes simplex virus 1 (HSV-1) thymidine kinase (HSV-TK) (Ray et al., 2004) (Figure 1A). We chose as a senescence-sensitive promoter that of the tumor suppressor p16<sup>INK4a</sup>, which has been used to track senescent cells in other mouse models (Baker et al., 2011; Burd et al., 2013; Yamakoshi et al., 2009). We engineered a bacterial artificial chromosome (BAC) containing approximately 50 kb of the murine p16<sup>INK4a</sup> locus such that the p16<sup>INK4a</sup> promoter drives 3MR expression. We inactivated the p16<sup>INK4a</sup> and adjacent p19-Arf genes in the BAC and created a transgenic mouse line (p16-3MR) containing a single integrated copy of the engineered BAC. Thus, p16-3MR mice are diploid for p16<sup>INK4a</sup> and p19-Arf. LUC allows the detection of 3MR-expressing cells by luminescence. mRFP permits sorting of these cells from tissues, and HSV-TK allows their killing by ganciclovir (GCV), a nucleoside analog that has a high affinity for HSV-TK but low affinity for the cellular TK. HSV-TK converts GCV into a toxic DNA chain terminator; in nondividing senescent cells, GCV fragments mitochondrial DNA, causing death by apoptosis (Laberge et al., 2013).

To verify 3MR transgene activity, we derived mouse embryonic fibroblasts (MEFs) from p16-3MR mice and induced the cells to senesce using X irradiation (IR; 10 Gy). As expected, endogenous p16<sup>INK4a</sup> protein levels increased, peaking ~10 days after IR (Figure S1A available online). We confirmed senescence by decreased DNA synthesis, increased SA- $\beta$ -gal activity (Figure S1B), increased levels of mRNAs encoding p16<sup>INK4a</sup>, p21, and the SASP factors interleukin-6 (IL-6) and MMP-3, and decreased levels of the mRNA encoding laminB1 (Freund et al., 2012) (Figure 1B). Importantly, mRNA levels encoding the 3MR transgene (mRFP) and endogenous p16<sup>INK4a</sup>, measured by quantitative PCR, behaved similarly (Figure 1B). Further, senescent p16-3MR MEFs expressed mRFP by

immunostaining (Figures 1C and S1B), with a concomitant increase in luciferase activity (Figure 1D). Finally, GCV selectively killed senescent p16-3MR MEFs and showed no significant toxicity in nonsenescent p16-3MR or wild-type (WT) cells (Figure 1E).

To verify that 3MR and endogenous p16<sup>INK4a</sup> were expressed similarly in vivo, we exposed p16-3MR mice to 7 Gy full-body IR. This IR dose is nonlethal but causes a persistent burden of senescent cells, which are evident 3 months later (Le et al., 2010). We treated the irradiated mice with GCV or PBS (vehicle control) 90 days after IR. IR induced luminescence in living animals (Figure 2A) and in isolated visceral fat, kidneys, and lungs (Figure S2A). These tissues also showed increased levels of mRNAs encoding p16<sup>INK4a</sup>, 3MR (mRFP), and the SASP factors IL-6 and MMP-3, but not the non-SASP factor IL-5 (Figures 2B, S2B, and S2C). Importantly, GCV treatment of irradiated p16-3MR mice markedly reduced total body luminescence and senescence-associated gene expression, but not IL-5 expression, in fat, kidneys and lungs (Figures 2A, 2B, S2B, and S2C).

Senescent cells increase with age in many tissues (Campisi, 2013). p16-3MR mice showed a significant increase in luminescence starting ~18 months of age (Figures S2D and S2E). GCV treatment of old (20–24 months) mice efficiently eliminated senescent cells as determined by reduced total body luminescence (Figures 2C and S2E) and reduced luminescence, SA- $\beta$ -gal staining, and p16<sup>INK4a</sup> mRNA levels in biopsies of visceral fat (Figures 2D–2F). Notably, visceral fat from young mice showed no difference in luminescence, SA- $\beta$ -gal, or p16<sup>INK4a</sup> mRNA levels upon GCV treatment (Figures 2D–2F).

Together, these findings show that p16-3MR transgenic mice accurately report the presence of senescent cells through luminescence and allow their elimination by GCV.

### Elimination of Senescent Cells Delays Cutaneous Wound Healing

Senescent stromal cells were shown to help resolve excessive fibrosis after skin or liver injury (Jun and Lau, 2010; Krizhanovsky et al., 2008). To directly assess the physiological consequences of cellular senescence during tissue repair, we analyzed the ability of p16-3MR mice to heal cutaneous wounds.

We administered small full-thickness punch biopsies to the dorsal flanks of p16-3MR mice. As reported by luminescence, senescent cells were detected transiently at the injury site. In young female p16-3MR animals, senescent cells were variable 2 days after wounding but significantly apparent 3 days after wounding; senescent cells peaked ~6 days after wounding and then returned to barely detectable basal levels between 9 and 12 days after wounding (Figures 3A and 3B). Male animals showed a similar transient induction of senescent cells but with kinetics that were slower by 2–3 days, consistent with their slower wound closure (Figure S3A). The induction of senescence after wounding was confirmed by the presence of RFP<sup>+</sup> (by immunostaining using an anti-RFP antibody since the fluorescent signal was lost after fixation) and SA- $\beta$ -gal<sup>+</sup> cells in the wound gap (Figures 3C and S3B). The levels of mRNAs encoding the senescence or SASP markers p16<sup>INK4a</sup>, mRFP, p21, IL-1 $\alpha$ , PAI-1, and vascular endothelial growth factor (VEGF) all increased and declined with kinetics similar to that of luminescence (Figures 3D–3F and S3C), confirming the transient presence of senescent cells during the wound healing process.

To determine the role of these transient senescent cells, we wounded 3- to 4-month-old p16-3MR mice and treated them with GCV 24 hours after injury. The effective elimination of senescent cells by GCV was confirmed by reduced luminescence (Figures 3A and 3B) and reduced mRNA levels encoding p16<sup>INK4a</sup>, mRFP, and p21 at the injury site (Figures 3D–3F). Strikingly, p16-3MR mice treated with GCV showed significantly delayed kinetics of wound closure compared with vehicle-treated p16-3MR or WT counterparts, with a peak delay at 6 days after wounding (Figures 3G and 3H). This finding indicates that the presence of senescent cells accelerates skin repair.

To independently confirm this finding, we analyzed p16<sup>INK4a</sup>/p21 double knockout mice (p16/p21 DKO). Cells from single p16<sup>INK4a</sup> or p21 KO mice are capable of senescence because of compensatory activities of p16<sup>INK4a</sup> and p21; however, cells from DKO mice show little or no senescence (Takeuchi et al., 2010). Similar to our findings using GCV-treated p16-3MR mice, p16/p21 DKO mice showed delayed wound healing compared with WT counterparts (Figure 3I). Importantly, wound healing in p16<sup>INK4a</sup> or p21 single knockout mice was similar to wound healing in WT mice (Figure 3I). Thus, the absence of p16<sup>INK4a</sup>- or p21-positive cells per se is not sufficient to delay wound healing. These data indicate that senescent cells facilitate cutaneous wound repair and that their absence significantly retards the kinetics of wound closure.

### Senescent Endothelial and Mesenchymal Cells Promote Granulation Tissue Formation

To understand how senescent cells contribute to wound healing and closure, we analyzed the wounds by histology 6, 9, and 15 days after injury. On day 6, the wounds of PBS-treated mice showed significant wound contraction and marked re-epithelialization. At this time, wounds of GCV-treated mice, in contrast, showed wide epithelial and dermal edges and the wound gap was filled with necrotic fibrinoid and cellular debris, with much reduced angiogenesis and inflammation, a paucity of collagen deposition, and poor formation of granulation tissue as revealed by trichrome staining (Figures 4A and 4B). Accordingly, GCV-treated wounds also showed a paucity of fibroblasts and endothelial cells (Figure 4A), consistent with impaired granulation tissue formation. Apoptosis was only slightly but not significantly increased in the poorly formed granulation tissue (Figure S4A), most likely reflecting the death of senescent cells and arguing against a significant bystander effect of GCV.

By 9 days after injury, granulation tissue formation and angiogenesis were similar between GCV- and vehicle-treated mice (Figure S4B), confirming a requirement for senescent cells for optimal kinetics of wound closure. However, 15 days after injury, wounds harbored by GCV-treated mice were significantly more fibrotic, as measured by collagen deposition and hydroxyproline content (Figures S4C–S4E), in agreement with reports indicating a role for senescent cells in limiting fibrosis in the skin and liver (Jun and Lau, 2010; Krizhanovsky et al., 2008). Analysis of the levels of mRNAs encoding different matrix metalloproteinases revealed that wound biopsies had significantly less MMP-2 but significantly more MMP-10 and MMP-13 when isolated from mice treated with GCV compared with vehicle-treated mice (Figure S4F). Moreover, dermal mouse fibroblasts showed reduced collagen production 6 days after we induced senescence by IR (Figure S4G). Thus, the senescent

cells in wounds likely secreted less collagen and expressed higher levels of certain MMPs, supporting our results with picrosirius red staining (Figure S4C) and a role for senescent cells in limiting fibrosis.

To determine the cell types that enter senescence after wounding, we sorted the RFP<sup>+</sup> population from skin biopsies 6 days after injury. Fluorescence-activated cell sorting analysis showed that RFP<sup>+</sup> cells comprised 2%–5% of the total cell population dissociated from the tissue (data not shown) and were senescent as determined by elevated expression of p16<sup>INK4a</sup>, p21, and 3MR mRNAs, decreased expression of lamin B1 mRNA (Figure 4C), and increased SA-β-gal positivity (Figure S4H). Notably, RFP<sup>+</sup> cells were positive for markers of fibroblasts and endothelial cells (which were highly enriched in the senescent population), but negative for keratinocyte markers (Figure 4D), indicating that fibroblasts and endothelial cells, but not the epidermal epithelial cells, are the predominant cell types that become senescent in response to skin injury. A fraction of senescent (RFP<sup>+</sup>) fibroblasts (2.8%) was also positive for a marker of myofibroblasts (smooth muscle actin [SMA]), as reported (Jun and Lau, 2010; Krizhanovsky et al., 2008).

To detect senescent cells in wounds independently of the 3MR transgene, we stained wound tissue for p21 (because, to date, we found that available antimouse p16 antibodies were not reliably specific). The kinetics of p21 expression were similar to that of p16<sup>INK4a</sup> and 3MR during wound closure (Figure 3F). Wound gaps of control, but not GCV-treated, mice showed p21<sup>+</sup> cells, which were mostly fibroblasts and capillary endothelial cells (based on morphology), confirming that senescent cells present in the wounds are mostly mesenchymal/fibroblastic and endothelial cells (Figure 4E).

### PDGF-A Is an Early SASP Factor Induced during Wound Healing

To define potential mechanisms by which senescent cells stimulate tissue repair, we isolated RFP<sup>+</sup> cells from wounds 6 days after injury and measured the levels of mRNAs encoding proteins known to aid in wound healing. Compared with RFP<sup>-</sup> cells, RFP<sup>+</sup> cells expressed very high levels of PDGF-A, not previously identified as a SASP factor, and VEGF, a known SASP component (Coppé et al., 2006) (Figure 5A). RFP<sup>+</sup> cells also had moderately elevated levels of the SASP factors PAI-1, CCL5, and CCL2, but not other SASP factors, such as IL-6 or transforming growth factor β (Figure 5A).

PDGF-A is expressed by several cell types during tissue repair and is generally reduced in mice with impaired wound healing (Beer et al., 1997). PDGF-A is also mitogenic for cells of mesenchymal origin that express the receptor PDGF-Rα, plays an important role in the formation of granulation tissue, and is crucial for myofibroblast differentiation/maturation during wound repair (Betsholtz, 2004; Boström et al., 1996; Ostman and Heldin, 2001; Pho et al., 2008).

*PDGFA*, but notably not *PDGFB*, mRNA increased between days 3 and 6 after wounding p16-3MR mice, and GCV strongly reduced *PDGFA* expression (Figures 5B and S5A). PDGF-A<sup>+</sup> cells were evident in the granulation tissue 6 days after wounding and were also RFP<sup>+</sup> (Figure 5C). In addition, RFP<sup>+</sup> mesenchymal and endothelial cells isolated from the wounds of p16-3MR animals were also PDGF-A<sup>+</sup> (Figure 5D). Further, cultured primary

mouse skin fibroblasts and endothelial cells expressed *PDGFA*, but not *PDGFB*, mRNA 4 days after they were induced to senesce by IR (Figures 5E and S5B). These senescent cells also secreted significantly higher levels of PDGF-AA, but not PDGF-AB or PDGF-BB, relative to nonsenescent cells (Figures 5F, S5C, and S5D). Thus, PDGF-AA is a SASP factor that is expressed by the senescent cells that populate wounds. This result was surprising because ectopic PDGF-BB, not PDGF-AA, is used clinically to enhance wound healing (Doukas et al., 2001).

In the 3–6 day interval after wounding, regardless of GCV treatment, the classic SASP factor IL-6 was not expressed (data not shown), although it was robustly induced 7–10 days after cultured MEFs were stimulated to senesce by IR (Coppé et al., 2008) (Figure S5E). In contrast, MEFs induced to senescence by IR expressed high levels of *PDGFA* mRNA very early (2–4 days) after the senescence stimulus (Figure S5E). These data suggest the SASP is a dynamic phenotype and that it can have different effects depending on the interval during which senescent cells are present.

### **Senescence-Associated PDGF-A Promotes Optimal Wound Closure through Myofibroblast Differentiation**

The speed of wound closure depends largely on wound contraction during the proliferative phase of wound healing (Midwood et al., 2004). This contraction is driven mainly by myofibroblasts, which are thought to arise from the conversion of wound site fibroblasts into a myofibroblastic phenotype (Gabbiani, 2003). Dermal fibroblasts isolated from p16-3MR mice and induced to senescence by IR showed no change in contractile capacity compared with nonsenescent fibroblasts, suggesting that senescent cells do not act cell autonomously during wound healing by directly contributing to contraction (Figure S6A). Notably, GCV strongly decreased the number of myofibroblasts in the midregion of p16-3MR wounds 6 days after injury (Figures 4A and S6B), as reflected by reduced SMA expression (Figure S6C). The paucity of myofibroblasts in senescence-free wounds was confirmed by decreased levels of the mRNA encoding cofilin, another marker of mature myofibroblasts (Figure S6D). Thus, elimination of senescent cells by GCV depleted wound sites of myofibroblasts, consistent with the slower wound healing shown by GCV-treated p16-3MR mice. Importantly, wounds with or without senescent cells showed comparable levels of Ki67<sup>+</sup> cells, arguing against a major effect of GCV on cell proliferation (data not shown).

Our findings suggest the PDGF-AA secreted by senescent fibroblasts and endothelial cells in wounded skin might optimize wound healing by inducing myofibroblast differentiation. In support of this idea, treatment of nonsenescent murine skin fibroblasts and MEFs with conditioned media from senescent cells increased the percentage of SMA-positive cells, similar to the increase obtained by treating the cells with recombinant PDGF-AA (Figures 6A and 6B; data not shown). This increase was suppressed by a PDGF-A blocking antibody, confirming that senescent cell-derived PDGF-AA was responsible for differentiating nonsenescent fibroblasts into myofibroblasts (Figures 6A and 6B).

To determine the physiological consequence of PDGF-AA secretion by senescent cells during wound healing, we topically applied recombinant PDGF-AA to skin wounds on p16-3MR mice in which senescent cells were eliminated by GCV. Strikingly, PDGF-AA

significantly increased the percentage of SMA-positive myofibroblasts in the wounds (Figures 6C and S6E) and completely restored the kinetics of wound closure to that of vehicle-treated mice (Figure 6D). Additionally, topical administration of the PDGF antagonist PDGF-RA delayed wound healing in the control mice, indicating that senescent cell-derived PDGF-AA is necessary and sufficient for timely wound closure in WT mice (Figure 6D). Wounds in p16-3MR mice treated with both GCV and PDGF-AA showed insignificantly reduced collagen deposition compared with wounds in PBS-treated mice (Figure S6F), suggesting that the increased fibrosis in senescence-free wounds is not due to a lack of PDGF-AA. As suggested by others, the increased fibrosis in senescence-free wounds might be due in part to the paucity of proteases secreted by senescent cells (Jun and Lau, 2010; Krizhanovsky et al., 2008).

Similar to GCV-treated p16-3MR mice, wounds in p16/p21 DKO mice showed significantly fewer myofibroblasts after wounding compared with WT mice (Figure S6G). Likewise, gene expression profiling revealed lower *PDGFA* mRNA levels in DKO tissues (Figure 6E), consistent with deficient myofibroblast differentiation and reduced granulation tissue formation. Importantly, as observed in GCV-treated p16-3MR mice, topical treatment with recombinant PDGF-AA rescued the delayed wound healing kinetics of p16/p21 DKO mice (Figure 6F). Topical PDGF-AA also had little effect on the fibrosis that developed after wounding p16/p21 DKO skin (Figure S6H).

Together, these findings identify PDGF-AA as an early SASP factor produced by senescent cells in wound sites, which optimizes myofibroblast differentiation and hence the kinetics of wound closure.

## DISCUSSION

Senescent cells accumulate with age and are thought to contribute to age-related diseases through the SASP (Coppé et al., 2008, 2010a; Krtolica et al., 2001; Parrinello et al., 2005). These deleterious effects do not explain why the cell nonautonomous phenotype of senescent cells was selected during evolution. However, recent reports showed a beneficial role for the SASP during embryonic development (Muñoz-Espín et al., 2013; Storer et al., 2013) and a role in limiting fibrosis after tissue injury (Jun and Lau, 2010; Krizhanovsky et al., 2008).

Our findings identify a positive effect of senescent cells and the SASP: the ability to accelerate cutaneous wound healing through the early secretion of the SASP factor PDGF-AA. Our data indicate that wounding induces senescence in resident fibroblasts and primarily endothelial cells. This senescence induction entailed the secretion of PDGF-AA by the senescent cells, which promotes myofibroblast differentiation, optimal granulation tissue formation, and ultimately the kinetics of wound closure.

The upstream signals that induce senescence after wounding are not yet known, although activation of the matricellular protein CCN1 was shown to induce senescence during skin and liver repair (Jun and Lau, 2010; Kim et al., 2013). Interestingly, CCN1 induced PDGF-A in primary cells in culture, but it also induced IL-6, a prominent late-appearing SASP

factor that we failed to identify as part of the senescence-associated repair program, at least during the transient appearance of senescent cells during wound healing (M.D. and J.C., unpublished data). Thus, CCN1 might only partially account for the senescence trigger. In agreement with previous findings (Jun and Lau, 2010; Krizhanovsky et al., 2008), we also found that the presence of senescent cells restrains fibrosis. While topical PDGF-AA compensated for the absence of senescent cells in GCV-treated p16-3MR and p16/p21 DKO mice with respect to the kinetics of wound closure, it did little to resolve the excess fibrosis, which is likely due to the absence of proteases that comprise the SASP.

In contrast to the well-documented deleterious effects of senescent cells and the SASP, the results presented here unambiguously demonstrate a positive role for senescent cells and the SASP in tissue repair. Notably, senescent cells were present only transiently during tissue repair, in contrast to the persistent presence of senescent cells in aged or chronically damaged tissues. Moreover, PDGF-A was induced very early upon senescence induction in cell culture, suggesting the time-dependent regulation of SASP factors might in part explain the beneficial versus deleterious effects of senescent cells. As such, our findings, together with several recent reports, help explain the evolutionary forces that shaped the complex senescence response. Future efforts are needed to determine possible differences among senescence inducers in consequent gene expression and protein secretion to better understand the dichotomy of how senescent phenotypes exert their effects in vivo.

## EXPERIMENTAL PROCEDURES

### Mice

p16-3MR mice (see Supplemental Experimental Procedures) were maintained in the AALAC-accredited Buck Institute for Research on Aging animal facility. All procedures were approved by the Institutional Animal Care and Use Committee. p16-3MR mice were bred in house.

For IR-induced senescence, 8-week-old p16-3MR mice were X irradiated (7 Gy) and treated 90 days later with vehicle or GCV. GCV was administered via daily intraperitoneal (i.p.) injections for 5 consecutive days at 25 mg/kg in PBS. Control mice were injected with an equal volume of PBS.

For wound healing, two equal-sized wounds were created on dorsal skin by a 6 mm punch. Treatment with GCV, PBS, recombinant PDGF-AA (BioVision; 20 ng topical applications), and PDGF-RA blocking peptide (Santa Cruz; 20 ng topical applications) were performed daily for 5 consecutive days before wounding or for 5 days starting 1 day after injury. Wound sizes were measured using a caliper.

### Cell Preparation and Culture

Day 13.5 embryos were dissected and cultured to produce MEFs, as described (Demaria et al., 2010). Skin fibroblasts were derived from the dorsal skin of 2- to 3-month-old mice, as described (Seluanov et al., 2010). Primary skin microvascular endothelial cells were purchased from Cellbiologics (Catalog No.: C57-6064) and cultured according to the manufacturer's protocol. For IR-induced senescence, cells were cultured to confluence,

exposed to 10 Gy X-rays, and analyzed 7, 10, or 15 days later; control cells were mock irradiated. For CCN1 treatments, recombinant protein (a gift from the Lester Lau laboratory) was diluted 1:20 in serum-containing medium and administered to cells for 3 days. Senescence was confirmed by bromodeoxyuridine labeling and SA- $\beta$ gal activity (Dimri et al., 1995) using commercial kits (Life Technologies and BioVision). Control and senescent cells were treated with the indicated concentrations of GCV for 6 days; the medium was refreshed every 2 days. Cell viability was assessed using the MTS assay (Promega) according to the manufacturer's protocol.

### **Bioluminescence**

For cell culture experiments, a Renilla Luciferase Assay System (Promega) was used according to the manufacturer's protocol; luminescence intensity was measured with a luminometer. For in vivo luminescence, mice were injected i.p. with 15  $\mu$ g of Xenolight RediJect Coelentarazine h (Calipers). At 25 min later, the mice were anesthetized with isoflurane, and luminescence was measured with a Xenogen IVIS-200 Optical in vivo imaging System (Caliper Life Sciences; 5 min medium binning).

### **Immunoblot Analysis**

Cells were washed with warm PBS, lysed, and subjected to SDS-PAGE using 4%–12% Bis-Tris gels; separated proteins were transferred to polyvinylidene fluoride membranes (Freund et al., 2012). Membranes were blocked and incubated overnight at 4°C with antirabbit primary antibodies (Santa Cruz Biotechnology for p16<sup>INK4a</sup>, actin, and tubulin; Abcam for SMA). Membranes were washed and incubated with horseradish peroxidase-conjugated (1:5,000; Cell Signaling) secondary antibodies for 45 min at room temperature and washed again. Signals were detected by enhanced chemiluminescence.

### **Real-Time PCR**

Total RNA was prepared using the PureLink Micro-to-Midi total RNA Purification System (Life Technologies). RNA was reverse transcribed into cDNA using a kit (Applied Biosystems). Quantitative RT-PCR (qRT-PCR) reactions were performed as described (Demaria et al., 2010) using the Universal Probe Library system (Roche). The *ACTIN* predeveloped TaqMan assay (Applied Bio-systems) was used to control for cDNA quantity. See Supplemental Information for a list of primers.

### **Enzyme-Linked Immunosorbent Assays, Conditioned Media, and Myofibroblast Differentiation**

ELISA kits to detect PDGF-AA, PDGF-AB, and PDGF-BB were from R&D Systems and used according to the manufacturer's protocols. Conditioned media were prepared by washing cells with serum-free Dulbecco's modified Eagle's medium (DMEM) and incubating in serum-free DMEM for 24 hr. ELISA results were normalized to cell number. For myofibroblast differentiation, conditioned media were supplemented with 2% fetal bovine serum before treating cells with blocking antibody against PDGF-A (200 ng/ml) or rabbit IgG (Santa Cruz Biotechnology). Recombinant PDGF-AA (20 ng/ml) was used as positive control.

## Histology

Formalin-fixed skin wound specimens were trimmed longitudinally along the wound center at the widest part of the wound (largest diameter area). Trimmed sections were processed, embedded in paraffin, blocked, sectioned, and stained with hematoxylin and eosin (H&E) and/or Masson's trichrome. Stained sections were examined histologically.

## Immunofluorescence

Cells or paraffin-embedded skin biopsies on glass coverslips were washed in PBS, fixed in 4% paraformaldehyde, quenched with 50 mM ammonium chloride, permeabilized with 0.3% Triton X-100 in PBS, saturated with 3% goat serum (Life Technologies), and incubated with primary antibodies at room temperature (Abcam, SMA; Santa Cruz, PDGF-A; Allele Biotechnology, mRFP) for 1 hr, followed by Alexa fluorescein-labeled secondary antibodies (Life Technologies) and Prolong Fade with 4',6-diamidino-2-phenylindole (DAPI) (Life Technologies). Images were quantified using ImageJ (<http://imagej.nih.gov/ij/>) and Cell Profiler ([www.cellprofiler.org](http://www.cellprofiler.org)).

## Immunohistochemistry

Sections were deparaffinized and rehydrated and then rinsed in 1 × Tris-buffered saline (TBS) for 10 min. Sections were microwaved in 10 mM citrate buffer for 5 min at 40% power in a 1,100 W oven and left to cool for 20 min. After a 10 min wash in 1 × TBS, endogenous peroxidase activity was blocked with 0.5% H<sub>2</sub>O<sub>2</sub> in 1 × TBS for 10 min; 10% normal goat serum was applied for 1 hr, and then VIMENTIN (Santa Cruz, at 1:30 dilution), FACTOR VIII (Deko, at 1:500), p21 (Santa Cruz, at 1:400), TUNEL (Millipore, at 1:300), and SMA antibodies (Abcam, at 1:100 in 1% bovine serum albumin [BSA]) were applied overnight. Sections were washed, incubated for 1 hr in biotinylated antirabbit antibody, diluted in 1% BSA in TBS (Vector Labs BA-1000 at 1:200), and then for 30 min with Vectastain Elite ABC reagent. Sections were washed and incubated using a 3,3'-diaminobenzidine (DAB) substrate kit for 4 min (Vector SK 4100). Sections were counterstained with hematoxylin and dehydrated. Slides were imaged using a Nikon E800 microscope. Hematoxylin and DAB staining were separated into two images using ImageJ Fiji and cells were counted using IMARIS spot count.

## Picrosirius Red Staining

Paraffin sections of skin biopsies were dewaxed and hydrated. Nuclei were stained with Weigert's hematoxylin for 8 min, and slides were washed for 10 min in running water and stained with picrosirius red solution for 1 hr (0.5 g Sirius Red, 500 ml saturated aqueous picric acid solution; Sigma-Aldrich). Slides were washed, dehydrated in 100% ethanol, cleared in xylene, and mounted in a resinous medium. Slides were examined through cross-polarized and bright field light, and positive areas were calculated using ImageJ.

## SA-β-Gal Assay

Skin biopsies were flash frozen in Optimal Cutting Temperature (OCT) and 10 μm sections cut. Immediately after sectioning, samples were fixed and stained overnight with an X-Gal solution using a commercial kit (Biovision). Samples were then mounted using Prolong with

DAPI. Images were acquired at 200× and 400× magnification, and the negative pictures of the SA-β-gal staining and DAPI images were merged.

### Hydroxyproline

Skin samples were collected 15 days after wounding, and conditioned media were collected after 24 hr of culture. Samples were analyzed using a commercial assay kit (Biovision). Briefly, 10 mg of tissue or 100 μl of conditioned media were hydrolyzed at 120°C for 3 hr, and 10 μl of each sample was evaporated to dryness and processed for optical density measurements using a colorimeter (560 nm).

### Contraction Assay

Control or irradiated skin fibroblasts ( $1.5 \times 10^5$ ) were plated on a 3D collagen matrix in 24-well plates (Cell Biolabs). At 48 hr later, the matrix was detached from the wells with a spatula; 2 hr later, contraction determined by measuring the diameter of the matrix using a ruler.

### Statistical Analysis

An unpaired t test was used to calculate a p value for pairwise comparisons; p values on multiple comparisons were calculated using two-way ANOVA with Bonferroni posttest.

### Supplementary Material

Refer to Web version on PubMed Central for supplementary material.

### Acknowledgments

We thank Cathy Vitelli, Shannon O'Hara, and Taki Te Koi for the help with histology, cell sorting, and imaging and Sanjiv Gambhir (Stanford University) for the 3MR construct. This work was supported by grants from the American Italian Cancer Foundation (M.D.), the Japan Science and Technology Agency (Presto to N.O. and Crest to E.H.), the U.S. NIH (AG017242 to H.V.S., J.C., J.H., J.V., M.E.T.D.; AG009909, AG041122, and CA166347 to J.C.), and a European Council Advanced Grant (GA233424 to J.H.).

### References

- Baker DJ, Wijshake T, Tchkonja T, LeBrasseur NK, Childs BG, van de Sluis B, Kirkland JL, van Deursen JM. Clearance of p16Ink4a-positive senescent cells delays ageing-associated disorders. *Nature*. 2011; 479:232–236. [PubMed: 22048312]
- Beer HD, Longaker MT, Werner S. Reduced expression of PDGF and PDGF receptors during impaired wound healing. *J Invest Dermatol*. 1997; 109:132–138. [PubMed: 9242497]
- Bethsholtz C. Insight into the physiological functions of PDGF through genetic studies in mice. *Cytokine Growth Factor Rev*. 2004; 15:215–228. [PubMed: 15207813]
- Boström H, Willetts K, Pekny M, Levéen P, Lindahl P, Hedstrand H, Pekna M, Hellström M, Gebre-Medhin S, Schalling M, et al. PDGF-A signaling is a critical event in lung alveolar myofibroblast development and alveogenesis. *Cell*. 1996; 85:863–873. [PubMed: 8681381]
- Burd CE, Sorrentino JA, Clark KS, Darr DB, Krishnamurthy J, Deal AM, Bardeesy N, Castrillon DH, Beach DH, Sharpless NE. Monitoring tumorigenesis and senescence in vivo with a p16(INK4a)-luciferase model. *Cell*. 2013; 152:340–351. [PubMed: 23332765]
- Campisi J. Cancer and ageing: rival demons? *Nat Rev Cancer*. 2003; 3:339–349. [PubMed: 12724732]
- Campisi J. Ageing, cellular senescence, and cancer. *Annu Rev Physiol*. 2013; 75:685–705. [PubMed: 23140366]

- Collado M, Blasco MA, Serrano M. Cellular senescence in cancer and aging. *Cell*. 2007; 130:223–233. [PubMed: 17662938]
- Coppé JP, Kauser K, Campisi J, Beauséjour CM. Secretion of vascular endothelial growth factor by primary human fibroblasts at senescence. *J Biol Chem*. 2006; 281:29568–29574. [PubMed: 16880208]
- Coppé JP, Patil CK, Rodier F, Sun Y, Muñoz DP, Goldstein J, Nelson PS, Desprez PY, Campisi J. Senescence-associated secretory phenotypes reveal cell-nonautonomous functions of oncogenic RAS and the p53 tumor suppressor. *PLoS Biol*. 2008; 6:2853–2868. [PubMed: 19053174]
- Coppé JP, Desprez PY, Krtolica A, Campisi J. The senescence-associated secretory phenotype: the dark side of tumor suppression. *Annu Rev Pathol*. 2010a; 5:99–118. [PubMed: 20078217]
- Coppé JP, Patil CK, Rodier F, Krtolica A, Beauséjour CM, Parrinello S, Hodgson JG, Chin K, Desprez PY, Campisi J. A human-like senescence-associated secretory phenotype is conserved in mouse cells dependent on physiological oxygen. *PLoS ONE*. 2010b; 5:e9188. [PubMed: 20169192]
- Demaria M, Giorgi C, Lebedzinska M, Esposito G, D'Angeli L, Bartoli A, Gough DJ, Turkson J, Levy DE, Watson CJ, et al. A STAT3-mediated metabolic switch is involved in tumour transformation and STAT3 addiction. *Aging (Albany NY)*. 2010; 2:823–842. [PubMed: 21084727]
- Dimri GP, Lee X, Basile G, Acosta M, Scott G, Roskelley C, Medrano EE, Linskens M, Rubelj I, Pereira-Smith O, et al. A biomarker that identifies senescent human cells in culture and in aging skin in vivo. *Proc Natl Acad Sci USA*. 1995; 92:9363–9367. [PubMed: 7568133]
- Doukas J, Chandler LA, Gonzalez AM, Gu D, Hoganson DK, Ma C, Nguyen T, Printz MA, Nesbit M, Herlyn M, et al. Matrix immobilization enhances the tissue repair activity of growth factor gene therapy vectors. *Hum Gene Ther*. 2001; 12:783–798. [PubMed: 11339895]
- Erusalimsky JD, Kurz DJ. Cellular senescence in vivo: its relevance in ageing and cardiovascular disease. *Exp Gerontol*. 2005; 40:634–642. [PubMed: 15970413]
- Freund A, Orjalo AV, Desprez PY, Campisi J. Inflammatory networks during cellular senescence: causes and consequences. *Trends Mol Med*. 2010; 16:238–246. [PubMed: 20444648]
- Freund A, Laberge RM, Demaria M, Campisi J. Lamin B1 loss is a senescence-associated biomarker. *Mol Biol Cell*. 2012; 23:2066–2075. [PubMed: 22496421]
- Gabbiani G. The myofibroblast in wound healing and fibrocontractive diseases. *J Pathol*. 2003; 200:500–503. [PubMed: 12845617]
- Guo S, Dipietro LA. Factors affecting wound healing. *J Dent Res*. 2010; 89:219–229. [PubMed: 20139336]
- Hayflick L, Moorhead PS. The serial cultivation of human diploid cell strains. *Exp Cell Res*. 1961; 25:585–621. [PubMed: 13905658]
- Jun JI, Lau LF. The matricellular protein CCN1 induces fibroblast senescence and restricts fibrosis in cutaneous wound healing. *Nat Cell Biol*. 2010; 12:676–685. [PubMed: 20526329]
- Kim KH, Chen CC, Monzon RI, Lau LF. Matricellular protein CCN1 promotes regression of liver fibrosis through induction of cellular senescence in hepatic myofibroblasts. *Mol Cell Biol*. 2013; 33:2078–2090. [PubMed: 23508104]
- Krishnamurthy J, Torrice C, Ramsey MR, Kovalev GI, Al-Regaiey K, Su L, Sharpless NE. Ink4a/Arf expression is a biomarker of aging. *J Clin Invest*. 2004; 114:1299–1307. [PubMed: 15520862]
- Krizhanovsky V, Yon M, Dickins RA, Hearn S, Simon J, Miething C, Yee H, Zender L, Lowe SW. Senescence of activated stellate cells limits liver fibrosis. *Cell*. 2008; 134:657–667. [PubMed: 18724938]
- Krtolica A, Parrinello S, Lockett S, Desprez PY, Campisi J. Senescent fibroblasts promote epithelial cell growth and tumorigenesis: a link between cancer and aging. *Proc Natl Acad Sci USA*. 2001; 98:12072–12077. [PubMed: 11593017]
- Laberge RM, Adler D, DeMaria M, Mechtouf N, Teachenor R, Cardin GB, Desprez PY, Campisi J, Rodier F. Mitochondrial DNA damage induces apoptosis in senescent cells. *Cell Death Dis*. 2013; 4:e727. [PubMed: 23868060]
- Le ON, Rodier F, Fontaine F, Coppe JP, Campisi J, DeGregori J, Laverdière C, Kokta V, Haddad E, Beauséjour CM. Ionizing radiation-induced long-term expression of senescence markers in mice is independent of p53 and immune status. *Aging Cell*. 2010; 9:398–409. [PubMed: 20331441]

- Martin JA, Buckwalter JA. The role of chondrocyte senescence in the pathogenesis of osteoarthritis and in limiting cartilage repair. *J Bone Joint Surg Am.* 2003; 85-A(Suppl 2):106–110. [PubMed: 12721352]
- Midwood KS, Williams LV, Schwarzbauer JE. Tissue repair and the dynamics of the extracellular matrix. *Int J Biochem Cell Biol.* 2004; 36:1031–1037. [PubMed: 15094118]
- Muñoz-Espín D, Cañamero M, Maraver A, Gómez-López G, Contreras J, Murillo-Cuesta S, Rodríguez-Baeza A, Varela-Nieto I, Ruberte J, Collado M, Serrano M. Programmed cell senescence during mammalian embryonic development. *Cell.* 2013; 155:1104–1118. [PubMed: 24238962]
- Noureddine H, Gary-Bobo G, Alifano M, Marcos E, Saker M, Vienney N, Amsellem V, Maitre B, Chaouat A, Chouaid C, et al. Pulmonary artery smooth muscle cell senescence is a pathogenic mechanism for pulmonary hypertension in chronic lung disease. *Circ Res.* 2011; 109:543–553. [PubMed: 21719760]
- Ohtani N, Yamakoshi K, Takahashi A, Hara E. The p16INK4a-RB pathway: molecular link between cellular senescence and tumor suppression. *J Med Invest.* 2004; 51:146–153. [PubMed: 15460900]
- Ostman A, Heldin CH. Involvement of platelet-derived growth factor in disease: development of specific antagonists. *Adv Cancer Res.* 2001; 80:1–38. [PubMed: 11034538]
- Parrinello S, Coppe JP, Krtolica A, Campisi J. Stromal-epithelial interactions in aging and cancer: senescent fibroblasts alter epithelial cell differentiation. *J Cell Sci.* 2005; 118:485–496. [PubMed: 15657080]
- Pho M, Lee W, Watt DR, Laschinger C, Simmons CA, McCulloch CA. Cofilin is a marker of myofibroblast differentiation in cells from porcine aortic cardiac valves. *Am J Physiol Heart Circ Physiol.* 2008; 294:H1767–H1778. [PubMed: 18263709]
- Ray P, De A, Min JJ, Tsien RY, Gambhir SS. Imaging trifusion multimodality reporter gene expression in living subjects. *Cancer Res.* 2004; 64:1323–1330. [PubMed: 14973078]
- Ressler S, Bartkova J, Niederegger H, Bartek J, Scharffetter-Kochanek K, Jansen-Dürr P, Wlaschek M. p16INK4A is a robust in vivo biomarker of cellular aging in human skin. *Aging Cell.* 2006; 5:379–389. [PubMed: 16911562]
- Seluanov A, Vaidya A, Gorbunova V. Establishing primary adult fibroblast cultures from rodents. *J Vis Exp.* 2010; (44)
- Sherr CJ, Roberts JM. CDK inhibitors: positive and negative regulators of G1-phase progression. *Genes Dev.* 1999; 13:1501–1512. [PubMed: 10385618]
- Storer M, Mas A, Robert-Moreno A, Pecoraro M, Ortells MC, Di Giacomo V, Yosef R, Pilpel N, Krizhanovsky V, Sharpe J, Keyes WM. Senescence is a developmental mechanism that contributes to embryonic growth and patterning. *Cell.* 2013; 155:1119–1130. [PubMed: 24238961]
- Takeuchi S, Takahashi A, Motoi N, Yoshimoto S, Tajima T, Yamakoshi K, Hirao A, Yanagi S, Fukami K, Ishikawa Y, et al. Intrinsic cooperation between p16INK4a and p21Waf1/Cip1 in the onset of cellular senescence and tumor suppression in vivo. *Cancer Res.* 2010; 70:9381–9390. [PubMed: 21062974]
- Tomasek JJ, Gabbiani G, Hinz B, Chaponnier C, Brown RA. Myofibroblasts and mechano-regulation of connective tissue remodelling. *Nat Rev Mol Cell Biol.* 2002; 3:349–363. [PubMed: 11988769]
- van Deursen JM. The role of senescent cells in ageing. *Nature.* 2014; 509:439–446. [PubMed: 24848057]
- Yamakoshi K, Takahashi A, Hirota F, Nakayama R, Ishimaru N, Kubo Y, Mann DJ, Ohmura M, Hirao A, Saya H, et al. Real-time in vivo imaging of p16Ink4a reveals cross talk with p53. *J Cell Biol.* 2009; 186:393–407. [PubMed: 19667129]

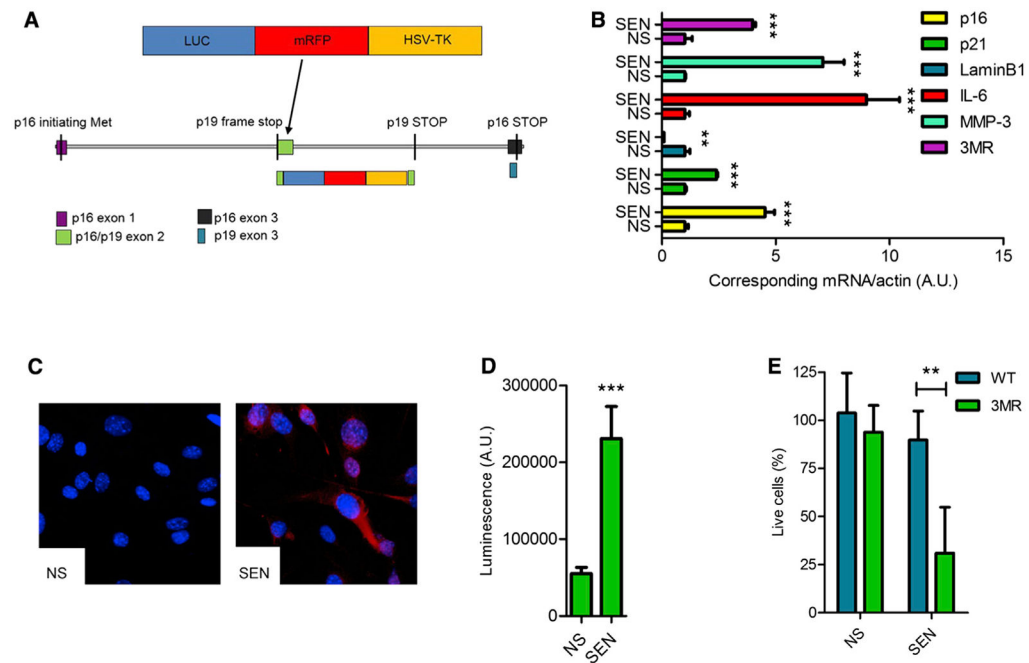


### Figure 1. Characterization of p16-3MR Cells

(A) Schematic of the p16-3MR transgene. See Results and Supplemental Experimental Procedures for details.

(B) qRT-PCR analysis of RNA isolated from nonsenescent (NS) and senescent (SEN; induced by 10 Gy IR) MEFs derived from p16-3MR embryos. RNA was analyzed for mRNA levels of the indicated genes relative to actin mRNA (control for cDNA quantity) ( $n = 3$  independent experiments; A.U., arbitrary units).

(C) Immunofluorescence of cells described in (B). Blue shows DAPI-stained nuclei; red shows mRFP immunostaining.

(D) Luminescence measurements of cells described in (B). Cells were incubated with coelenterazine and lysed, and luminescence intensity was quantified using a luminometer ( $n = 3$ ; A.U., arbitrary units).

(E) WT or p16-3MR MEFs were treated with GCV (10  $\mu\text{g/ml}$ ) for 7 days and evaluated for the percentage of surviving cells using the MTS assay ( $n = 4$ ).

Data shown are the mean  $\pm$  SD. \*\* $p < 0.01$ , \*\*\* $p < 0.001$ .

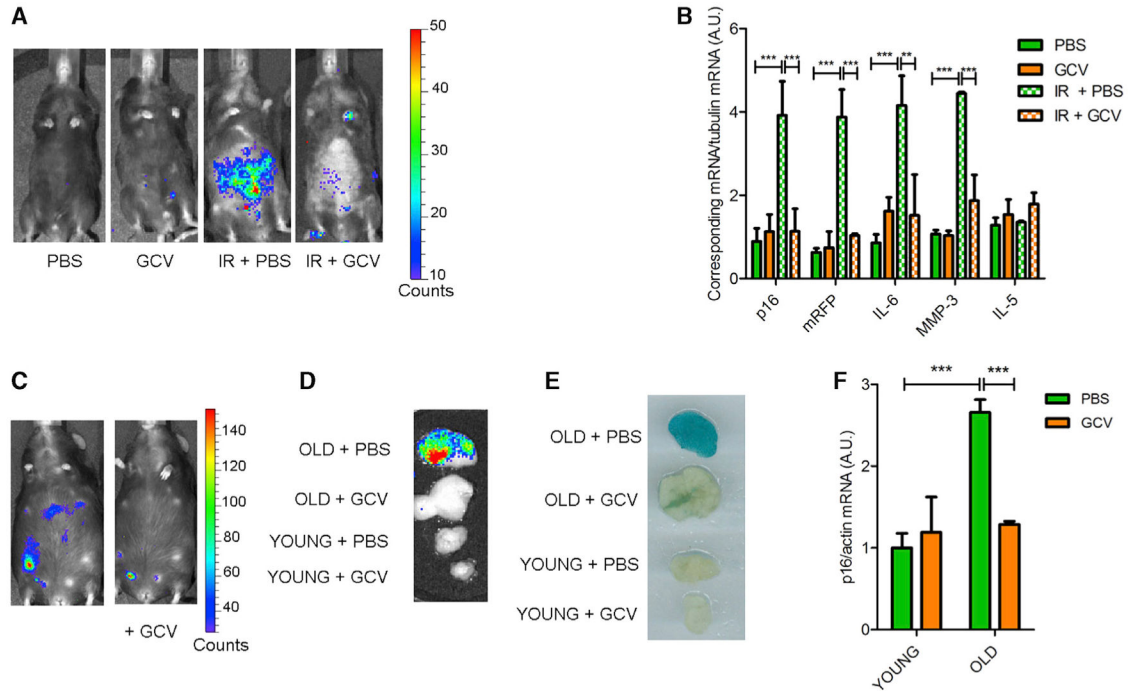


### Figure 2. Characterization of p16-3MR Mice

(A) Mock or IR p16-3MR mice, treated with vehicle (PBS) or 25 mg/kg of GCV for 5 days (daily i.p. injections; GCV), were injected with coelenterazine, and luminescence was quantified using a Xenogen Imaging system.

(B) RNA was extracted from the fat of mice described in (A) and quantified by qRT-PCR for mRNA levels of endogenous p16<sup>INK4a</sup>, mRFP, IL-6, MMP-3, and IL-5. Tubulin mRNA was used as a control (n = 4).

(C) Representative image of a 24-month-old p16-3MR mouse before (left) and after (right) GCV treatment. Luminescence was quantified using a Xenogen Imaging system.

(D–F) Fat biopsies from old (20–24 months) or young (3–4 months) p16-3MR mice, treated with PBS or GCV as described in (A). (D) Biopsies were incubated with a coelenterazine solution and luminescence quantified using a Xenogen Imaging system. (E) Biopsies were fixed in formalin, stained at pH 6 with X-Gal solution to measure SA- $\beta$ -gal activity, and recorded using a photoscanner. (F) RNA was extracted from the biopsies and quantified by qRT-PCR for mRNA levels of endogenous p16<sup>INK4a</sup>. Actin mRNA was used as a control (n = 4).

Data show are the mean  $\pm$  SD. \*\*p < 0.01; \*\*\*p < 0.001.

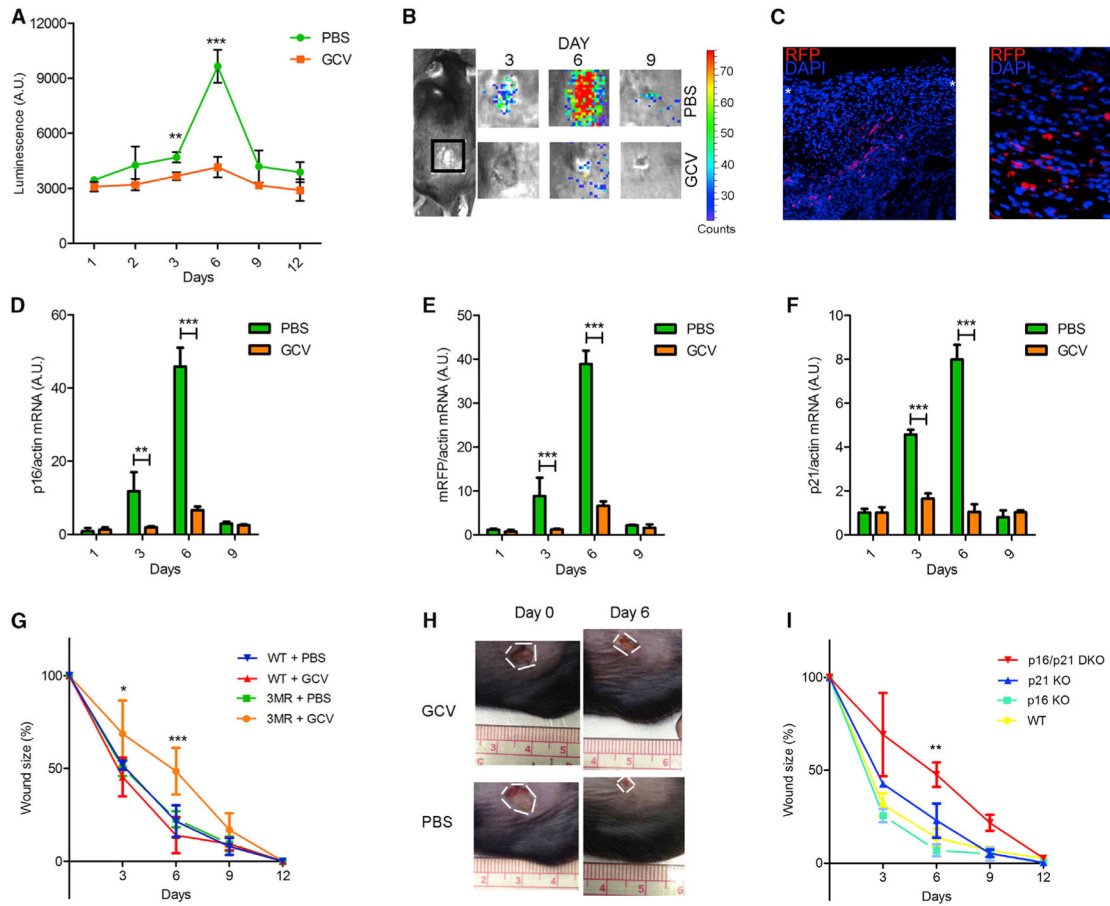


### Figure 3. Senescent Cells Are Induced and Necessary for Optimal Cutaneous Wound Healing

In all cases, mice were wounded using a 6 mm punch to dorsal skin and treated with PBS (vehicle control) or GCV (five daily i.p. injections) from 1 to 6 days after injury (n = at least 4 mice per group).

(A and B) p16-3MR mice were wounded, injected i.p. with coelenterazine, and imaged with a Xenogen imaging system at the indicated times after injury. (A) Quantification of the luminescence. (B) Typical images, both at the indicated time (days) after injury.

(C) Skin biopsies of p16-3MR mice were collected 6 days after injury, fixed, and stained for nuclei (DAPI; blue) or mRFP (immunostaining; red). White asterisks define the wound edges.

(D–F) p16<sup>INK4a</sup> (D), mRFP (E), and p21 (F) mRNA levels were quantified by qRT-PCR from skin biopsies excised from PBS or GCV-treated wounds to p16-3MR mice at the indicated intervals after injury. Actin was used to control for cDNA quantity.

(G) Wound sizes of WT or p16-3MR mice were measured at the indicated days after wounding.

(H) Representative image of wounds at the indicated days after injury of p16-3MR mice.

(I) Wound sizes of WT, p16 KO, p21 KO, and p16/p21 DKO mice were measured at the indicated days after wounding.

Data shown are the mean  $\pm$  SD. \*p < 0.05, \*\*p < 0.01, \*\*\*p < 0.0001.

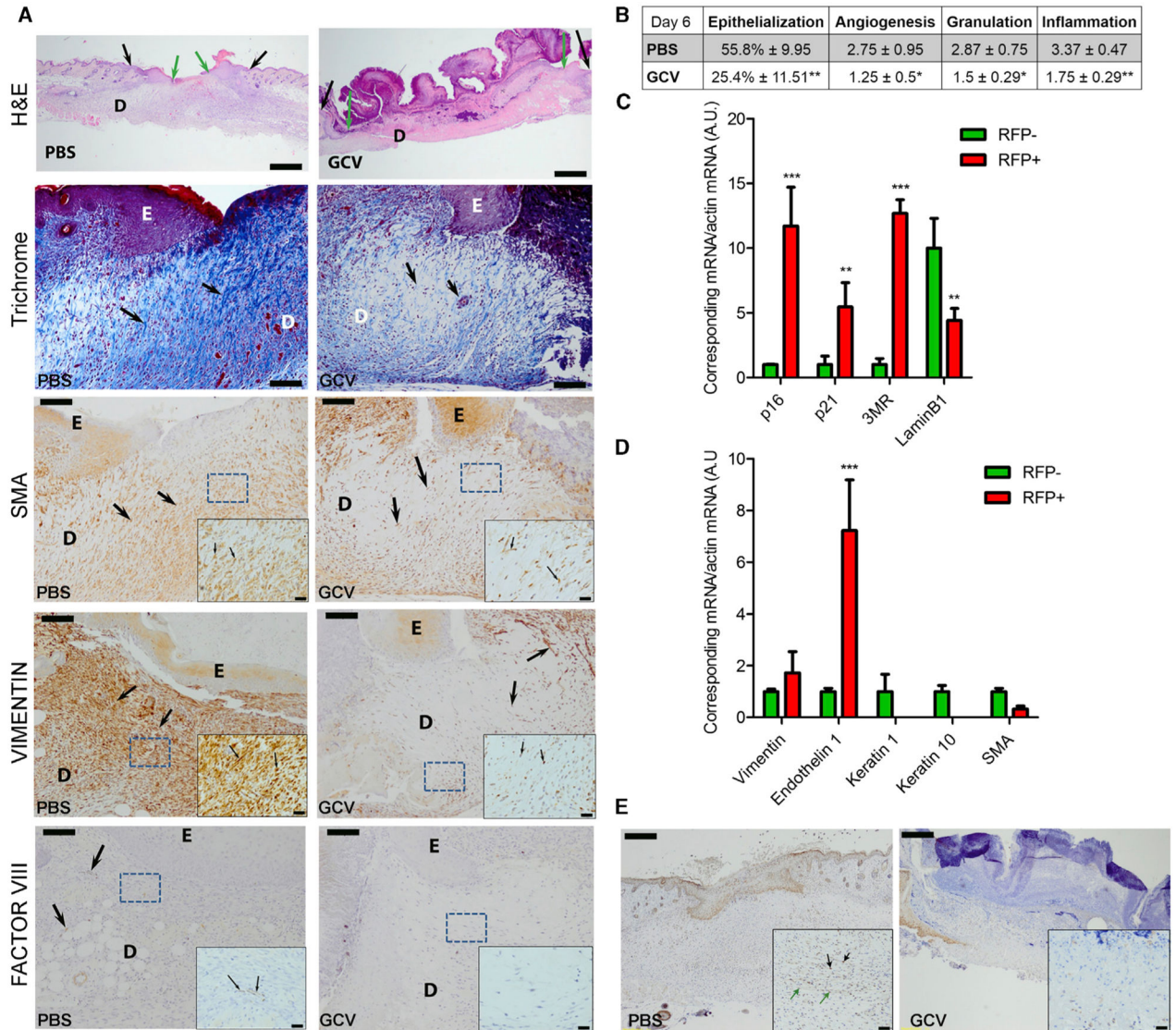


#### Figure 4. Characterization of Senescent Cells Induced during Wound Healing

(A) Longitudinal sections of wounds from PBS-treated (vehicle, left panels) and GCV-treated mice (right panels) ( $n = 8$ ), collected 6 days after wounding, were stained with H&E or specific antibodies and scored. Dermis is defined as D and epidermis as E. In the H&E staining, black and green arrows indicate the original wound edges and re-epithelialized edges, respectively. Scale bars represent 500  $\mu\text{m}$ . Sections were additionally stained with Masson's trichrome (for collagen fibers) or antibodies against SMA (marker for myofibroblast), vimentin (marker for mesenchymal cells), or factor VIII (marker for endothelial cells). Higher magnification of the boxed areas is shown on the bottom to the right. Positive staining is indicated by arrows. Scale bars represent 100  $\mu\text{m}$  for the main panel and 20  $\mu\text{m}$  for the insets.

(B) Table shows the percentage of epithelialization after injury and histological scores for angiogenesis, granulation, and inflammation, based both on the staining represented in (A).

(C and D) Cells from wounds collected 6 days after injury were isolated and sorted for RFP. mRNA levels encoding the indicated proteins were quantified by qRT-PCR. Actin was used as a control for RNA quantity (n = 3 independent experiments).

(E) Sections described in (A) were immunostained for p21. Black arrows indicate positive fibroblasts, and green arrows indicate positive endothelium. Insets show higher magnification of the section. Scale bars represent 200  $\mu\text{m}$  for the main panel and 40  $\mu\text{m}$  for the insets. Data shown are the mean  $\pm$  SD. \*p < 0.05, \*\*p < 0.01, \*\*\*p < 0.0001.

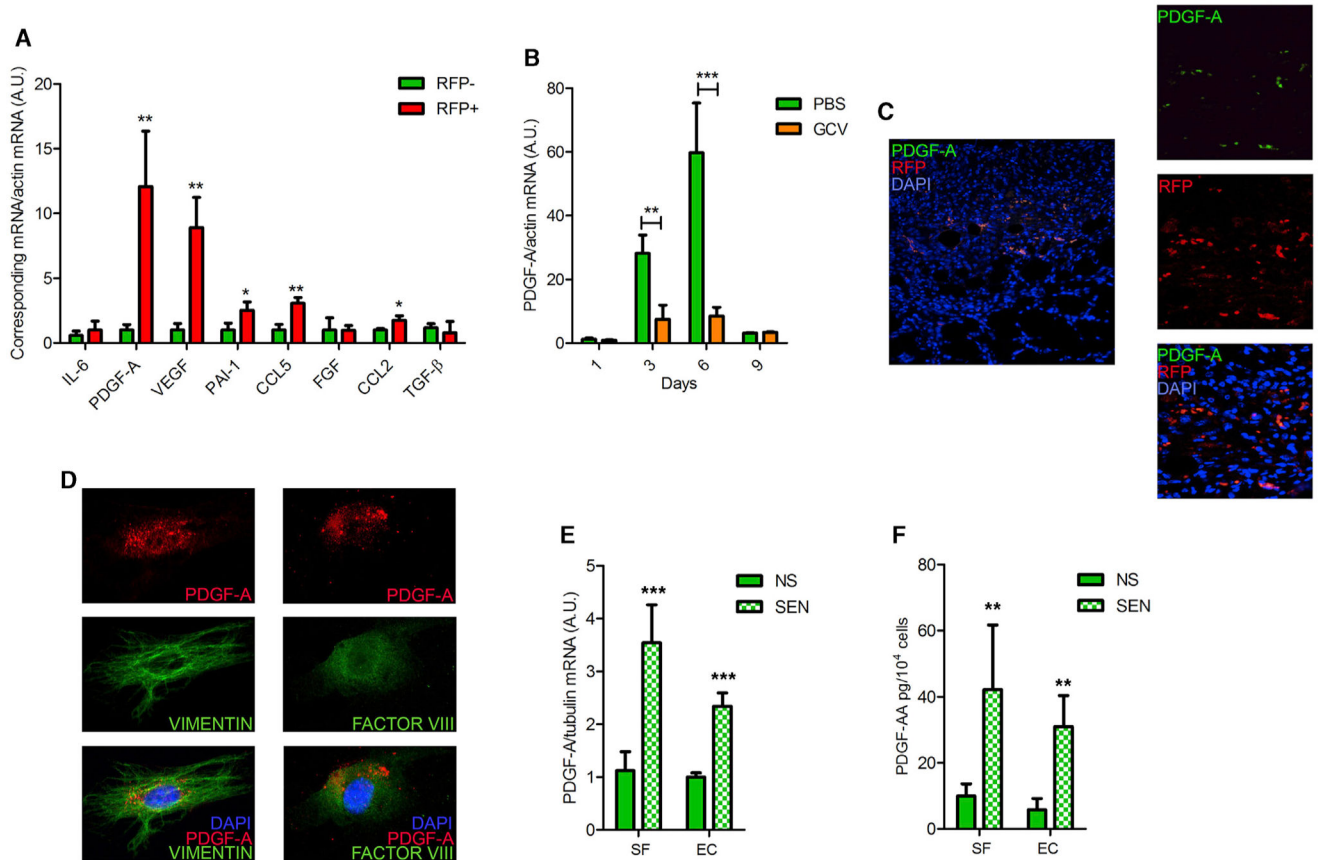


### Figure 5. PDGF-A Is Expressed and Secreted by Senescent Cells

(A) mRNA levels of the indicated proteins were quantified by qRT-PCR in cells sorted from wounds as described in Figure 4D. Actin was used to control for RNA quantity (n = 3).

(B) Skin biopsies excised from PBS- or GCV-treated wounds in p16-3MR mice were collected at the indicated intervals after injury, and PDGFA mRNA levels were quantified by qRT-PCR. Actin was used to control for RNA quantity (n = 5).

(C) Skin biopsies of p16-3MR mice were collected 6 days after injury, fixed, stained with DAPI (blue; indicating nuclei), and immunostained for mRFP (red) and PDGF-A (green).

(D) Cells were derived from wounds 6 days after injury and sorted for RFP. RFP<sup>+</sup> cells were plated, fixed 24 hr later, and then stained with DAPI (blue) and immunostained for PDGF-A (red) and vimentin (green, left panels) or factor VIII (green, right panels).

(E and F) Murine skin fibroblasts (SF) or endothelial cells (EC) were mock irradiated (NS) or made senescent by irradiation (SEN; 10 Gy X-ray). At 4 days after irradiation, RNA and conditioned media were collected and analyzed for PDGF-A mRNA and secreted protein by qRT-PCR and ELISA, respectively (n = 4). Data shown are the mean  $\pm$  SD. \*p < 0.05, \*\*p < 0.01, \*\*\*p < 0.0001.

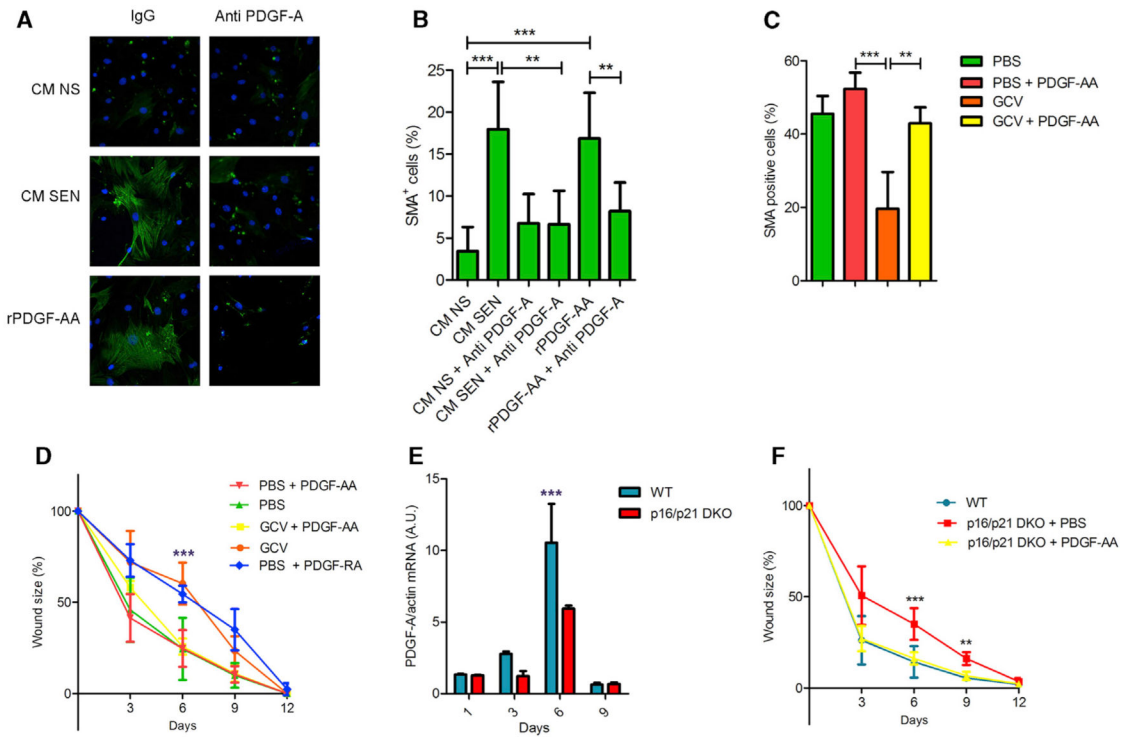


### Figure 6. Senescence-Associated PDGF-A Drives Myofibroblast Differentiation

(A and B) Skin fibroblasts were incubated with conditioned media from IR-induced senescent (CM SEN) or nonsenescent (CM NS) cells containing nonspecific rabbit IgG or a PDGF-A blocking antibody; after 48 hr, the cells were immunostained for SMA (green), and nuclei were stained with DAPI (blue). Ten ng/ml recombinant PDGF-AA was used as a positive control. (A) Representative image. (B) Percentage of SMA-positive cells relative to the total (DAPI positive) number of cells ( $n = 6$ ).

(C and D) Wound healing was performed as described in Figure 3G, except PDGF-AA (20 ng) or vehicle (PBS) were topically applied daily from 1 to 6 d after wounding ( $n = 5$ ). (C) Biopsies from wounds 6 days after injury were embedded in paraffin and stained for SMA. The graph shows the percentage of positive cells present in the wound gap. (D) Wound sizes were measured at the indicated times after injury. In addition to the groups described, a cohort of control p16-3MR mice was treated with PDGF-RA (daily topical application of 20 ng from 1 to 6 days after injury).

(E) RNA was isolated from wounded areas 6 days after injury of WT and p16/p21 DKO mice. PDGFA mRNA levels were quantified by qRT-PCR. Actin was used to control for RNA quantity ( $n = 3$ ).

(F) Wound healing was performed and measured as described in (B). PDGF-AA (20 ng) or vehicle (PBS) were topically applied daily from 1 to 6 days after wounding ( $n = 3$ ). Data shown are the mean  $\pm$  SD. \*\* $p < 0.01$ , \*\*\* $p < 0.0001$ .